Catalysis Today 176 (2011) 340–346

Contents lists available at ScienceDirect

Catalysis Today

journal homepage: www.elsevier.com/locate/cattod

Alumina-supported nickel catalysts for catalytic partial oxidation of methane in short-contact time reactors

Luigi D. Vella, Stefania Specchia*

Department of Materials Science and Chemical Engineering, Politecnico di Torino, Corso Duca degli Abruzzi 24, 10129 Torino, Italy

ARTICLE INFO

Article history:
Available online 28 December 2010

Keywords:
Syngas
Methane catalytic partial oxidation
Short contact time
Fixed bed reactor
Ni catalyst
Alumina carrier

ABSTRACT

The aim of this work was the development and performance evaluation of alumina supported nickel catalysts for partial oxidation of methane to syngas in a self-sustained short contact time fixed bed reactor using pure oxygen or air. It was also verified the attainment of relative constant temperatures in an appropriate range (750–1050 °C) along the catalytic fixed bed independently of the operative weight hourly space velocity (WHSV); thus sintering and coking problems and the consequent performance decay were avoided. The activity tests with a Ni load of 5% and 10% by weight were carried out increasing the WHSV from 150 to 1440 Nl h^{-1} $g_{cat}{}^{-1}$. The results obtained with 10% Ni/Al_2O_3 catalyst when working with pure O_2 showed an excellent performance towards CH_4 conversion (>90%) and H_2 selectivity (>95%), comparable to the best rhodium based catalysts tested at the same operating condition [29]. When working with air, 10% Ni/Al_2O_3 was able to maintain the reactor thermally self-sustained using air rather than pure oxygen until WHSV of 1440 Nl h^{-1} $g_{cat}{}^{-1}$ (GHSV ≈ 750,000 h^{-1}) and gave a performance similar to that with pure O_2 (but producing a syngas diluted by N_2) till a WHSV value of about 600 Nl h^{-1} $g_{cat}{}^{-1}$.

1. Introduction

The energy increasing demand of the modern society stimulates exploration of new energy technologies. Partial oxidation is presently considered an alternative to steam reforming for the generation of H_2 from fossil fuels in decentralized applications [1] and for stationary or mobile fuel cells [2]. The catalytic partial oxidation (CPO) of CH_4 to CO/H_2 mixtures has been largely discussed; several catalysts were proposed, including non-noble [3,4] and noble metals based ones [5,6]. The main chemical reactions involved in the catalytic process are exothermic reactions (CH_4 total and partial oxidation, water gas shift equilibrium, coke formation according to Boudouard equilibrium) and endothermic reactions (steam and dry reforming) [7].

The extensive work on short contact-time (SCT) reactors [8–17] showed Rh highly active and selective, superior to other noble metals, able to avoid or at least partially limit coke formation [18]. It is widely accepted that with metal catalysts CH_4 is firstly oxidized to CO_2 and H_2O in the initial part of the catalytic bed until O_2 is exhausted [19]; then the reforming reactions of remaining CH_4 with steam and CO_2 initially formed occur [5,6]. However, at extremely high temperatures and very short contact time, syngas may be formed directly [6–9]. It has been reported, in fact, that the development of the combustion-reforming or direct reaction mechanism depends also on the interaction between the active element and the support: Weng et al. [20] studying the CPO of methane with Rh-based catalysts on two different supports found that the direct reaction to syngas was the main pathway over Rh/SiO_2 catalyst whereas combustion-reforming was the dominant one over $Rh/\gamma\text{-}Al_2O_3$ catalyst. They suggested as responsible for the significant difference in the reaction mechanisms the variation in the surface concentration of oxygen species over the catalysts under the reaction conditions, mainly due to the unlike affinity between oxygen and Rh species on the two supports.

The very active and stable Rh catalysts employ, however, a very expensive noble metal, whose price fluctuates significantly [21]. Cheaper and alternative metal-based catalysts (such as Fe-, Co-, and Ni-based ones) would be desirable. In particular, Ni catalysts have been widely investigated because of their low cost and relatively high activity in methane CPO. Dissanayake et al. [6] reported for Ni/Al_2O_3 nearly complete conversion of CH_4 with 95% CO selectivity at reaction temperatures above 700 °C by using an excess of O_2 compared to the stoichiometric requirements. Conversely, the catalyst suffered deactivation by carbon deposition. Other drawbacks, such Ni particles sintering [22,23] and phase transformation of the carrier [24], have also been reported for Ni-based catalysts in CH_4 CPO. Nonetheless, these catalysts have been widely studied because of their high catalytic activity and economic advantages.

Concerning the reaction mechanisms over nickel, Liu et al. [25] claimed that in well reduced $Ni/\theta\text{-}Al_2O_3$ catalysts characterized by

* Corresponding author. Tel.: +39 011 0904608; fax: +39 011 0904699.
E-mail address: stefania.specchia@polito.it (S. Specchia).

0920-5861/$ – see front matter © 2010 Elsevier B.V. All rights reserved.
doi:10.1016/j.cattod.2010.11.068

high activity towards CH_4 dissociation, both metallic nickel and NiO_x ($x < 1.0$) performed as active phases for partial oxidation of CH_4, which could be partially oxidized to CO and H_2 by the lattice oxygen of NiO_x. The bond strength of Ni–O seemed to act favourably to CH_4 partial oxidation, most likely due to the strong interaction between NiO_x and θ-Al_2O_3. However, Dissanayake et al. [6] suggested the presence in a fixed bed of irregular Ni/Al_2O_3 particles, in contact with an O_2–CH_4 mixture in the molar ratio of 0.56, of three different regions: in the first region, the inlet one contacted by CH_4/O_2 fed mixture, they detected the presence of the spinel $NiAl_2O_4$, which had only moderate activity for the methane complete oxidation to CO_2 and H_2O. In the intermediate region they identified the NiO + Al_2O_3 phase, over which complete oxidation of CH_4 to CO_2 and steam occurred. As a result of the complete O_2 consumption in the second region, the reduced Ni/Al_2O_3 phase in the third portion of the catalyst bed allowed the formation of the final CO and H_2 products, via reforming reactions of the residual CH_4 with the CO_2 and H_2O produced during the complete methane oxidation over the NiO/Al_2O_3 phase. Very recently, Özdemir et al. [26] demonstrated how the support basicity greatly influenced both the H_2/CO ratio and the carbon deposition: H_2/CO decreased gradually by increasing the basicity level, which in turns enhanced the reverse WGS and the reverse Boudouard reaction. Carbon deposition, in fact, decreased in the order: Al_2O_3 > MgO/Al_2O_3 > $MgAl_2O_4$ > MgO.

The present work reports the preparation, characterization, and catalytic performance evaluation of Ni-based catalysts, namely 5% and 10% Ni, over γ-Al_2O_3 irregular particles. The main goal was the development of suitable catalysts able to maintain the temperatures in the fixed bed in an appropriate range (750–1050 °C) independently of the operative feed gas flow rates, avoiding thus sintering and coking problems and limiting the consequent performance decay. Both pure O_2 and air were used as reactant feedstock.

2. Experimental

Two different Ni based catalysts (5% Ni/Al_2O_3 and 10% Ni/Al_2O_3) were prepared by Ni deposition over γ-Al_2O_3 irregular particles obtained by crushing and sieving commercial alumina spheres (3 mm in diameter, Sasol Germany GmbH); the fraction 600–1000 μm was used. Ni was deposited by incipient wetness impregnation technique at room temperature, using nickel (II) nitrate hexahydrate (Aldrich) dissolved in isopropyl alcohol. The as-prepared particles were left at rest overnight and then placed in oven with a temperature ramp of 5 °C min^{-1} until 900 °C and at this temperature calcined in calm air for 2 h.

The catalysts' morphology was observed by field emission scanning electron microscopy (FESEM FEI Quanta Inspect 200 LV apparatus, coupled with EDAX GENESIS SUTW-sapphire detector).

The specific surface area (s.s.a.) and pore size distribution (p.s.d.) were measured via N_2 adsorption at the liquid N_2 temperature with an automated gas sorption analyzer (Micromeritics ASAP 2010 M apparatus), by degassing in vacuum for at least 12 h at 300 °C before analysis. The s.s.a. was determined according to the BET theory method within the relative pressure range 0.05–0.3. The p.s.d. was determined by using the BJH method calibrated for cylindrical pores. Metallic Ni dispersion on the carrier was estimated by CO chemisorption at 40 °C with the same apparatus employed for BET s.s.a. and BJH p.s.d.: prior to the experiments, the catalysts were reduced at 350 °C for 2 h by flowing H_2 at a rate of 20 N cm^3 min^{-1} and then degassed firstly at 350 °C for 2 h and afterwards at 40 °C for 0.5 h. The chemisorbed CO was determined by extrapolation to zero pressure of the linear part of the adsorption isotherm after removing the so-called reversibly adsorbed CO ("double isotherm" procedure) and assuming a chemisorption stoichiometry Ni:CO = 1:1.

XRD analysis measurements were recorded with Philips PW1710 apparatus equipped with a monochromator for the Cu Kα radiation.

XPS analysis measurements were recorded using a PHI 5000 VERSA PROBE spectrometer equipped with a hemispherical electron analyzer and an Al Kα ($h\upsilon$ = 1486.6 eV) 25.6 W X-ray source. The peaks' area was estimated by each peak integration after smoothing and subtraction of an S-shaped background and fitting of the experimental curve to a mixture of Lorentzian and Gaussian lines of variable proportions. All binding energies (BE) were referenced to the C 1s signal at 284.6 eV from carbon contamination of the samples to correct the charging effects. The atomic fractions on the sample surface were quantified by peaks' integration with appropriate corrections for sensitivity factors [27].

The catalytic activity of the prepared catalysts was determined in a fixed bed reactor, already fully described in [28,29]. Briefly, CH_4 and O_2 (or air), mixed at room temperature, were fed to the reactor (an Inconel 601 tube of 12 mm i.d. and 2 mm wall thickness with the internal surface covered by a layer of oxidized FeCrAlloy to avoid any contact between the reactive gases and the alloy wall, just to prevent any catalytic effect of Ni present in the latter). For safety reasons, pure N_2 (technical grade, rate 2 Nl min^{-1}) was used to fill up the reactor before and after each test. The catalyst fixed bed was arranged between two inert fixed beds: upstream, quartz particles (to complete the reagents static mixing) were followed by high thermal conductivity SiC particles, to provide a shield for the radiant energy emerging from the catalytic zone and promote reagents preheating. Downstream, low thermal conductivity quartz particles reduced heat losses and cooled slowly the outlet stream. The gas temperatures were monitored by thermocouples located at catalytic bed inlet and outlet. The outlet gas stream composition was determined by a multiple gas analyzer (ABB), for H_2 (thermal conductivity analyzer module Caldos 17), CO/CO_2/CH_4 (infrared analyzer module Uras 14), and O_2 (paramagnetic O_2 analyzer module Magnos 106) concentrations. For safety and environment protection reasons, after the analysis section, the produced syngas was completely oxidized by a catalytic honeycomb burner.

The reactor was heated up to 920 °C in a tubular oven by feeding N_2 (2 Nl min^{-1}). Then, the CPO reaction was ignited feeding a room temperature mixture of pure CH_4 and O_2 or CH_4 and air at O_2/CH_4 ratio slightly above the stoichiometry (operative average values: 0.572 ± 0.005 for tests with pure O_2 [28,29]; 0.606 ± 0.008 for tests with air) to provide enough thermal input to the reactor. Once ignited the catalytic bed, the oven was switched off as the SCT-CPO reaction resulted thermally self-sustained by the heat released in the reaction zone. The ignition procedure was very quick taking about 1 min. The feed flow rate was adjusted accordingly to increase the weight hourly space velocity WHSV (i.e., the ratio between the flow rate and the catalyst mass in the reactor) from 170 to 600 Nl h^{-1} g_{cat}^{-1} when pure O_2 was used, or from 200 to 1440 Nl h^{-1} g_{cat}^{-1} when air was used. The CH_4 flow rate fed to the reactor, i.e., the potential overall thermal power input to the reactor, was the same for both the test runs (O_2 or air). The prepared catalysts were tested by placing in the reactor ~1.2 g, to form a fixed bed with ~20 mm of axial length.

3. Results and discussion

FESEM analysis of the as-prepared 5% Ni/Al_2O_3 (Fig. 1A and C) pointed out the morphology of the alumina support used in the catalyst preparation; spongy and porous Al_2O_3 structures were present and at high magnification it was possible to see a long and narrow leaf-shape structure. FESEM analysis showed the same morphology for 10% Ni/Al_2O_3 (Fig. 1B and D), also as concerns the

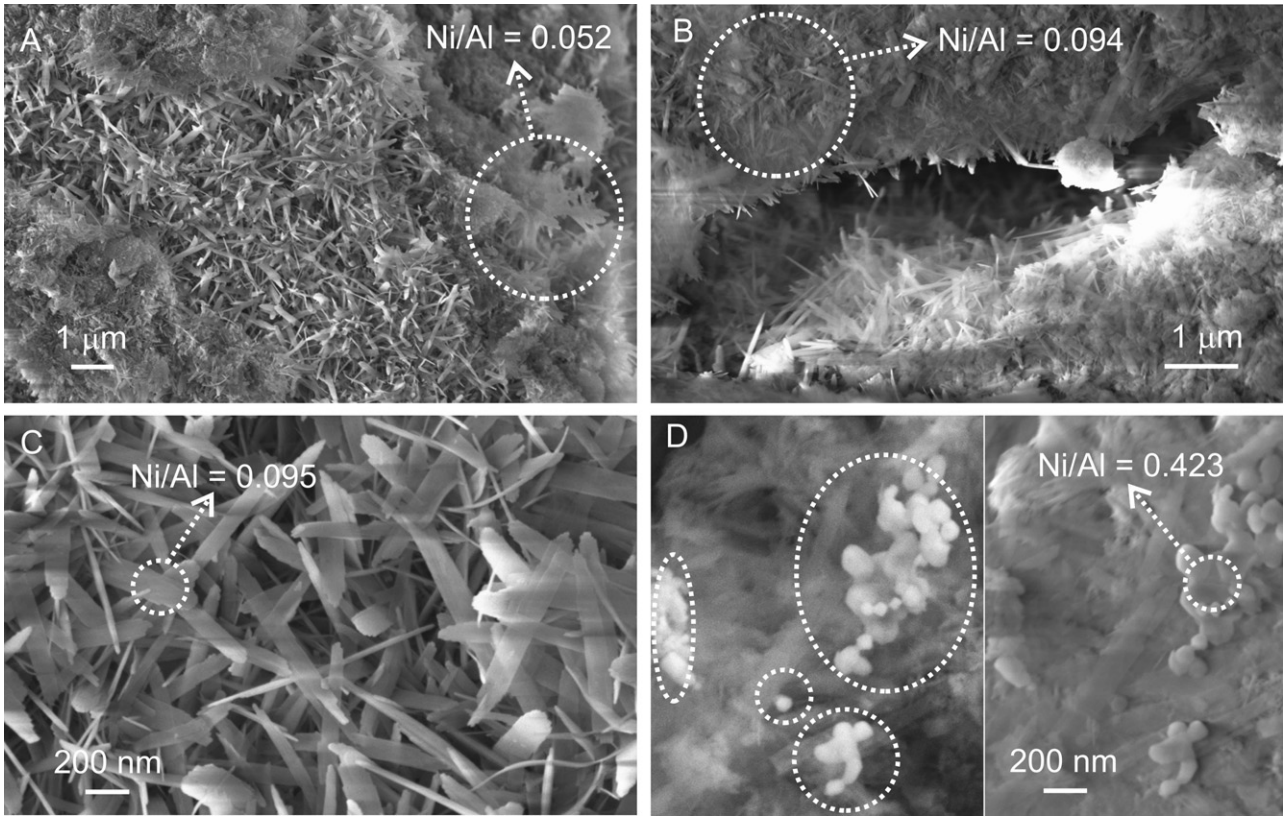

Fig. 1. FESEM images of the 5% Ni/Al_2O_3 (A and C) and 10% Ni/Al_2O_3 (B and D) catalysts at various magnifications. Ni clusters of 10% Ni/Al_2O_3 are enlightened (backscattered image). Atomic Ni/Al ratios calculated from EDX spectra in the enlightened zones are reported.

like leaf-shape structure, but for this catalyst FESEM investigation revealed a widespread presence of numerous bright spots of various sizes (the larger ones up to 100 nm approximately), constituted by Ni crystallite aggregates directly exposed on the catalytic surface particles. The amount and sizes of Ni crystallites probably would increase with the Ni load on the catalyst; anyway, nickel bright spots were not present on 5% Ni/Al_2O_3. This occurrence could be due to the fact that Ni deposit was diluted in the matrix carrier or chemically bonded with it, as evidenced by the XPS analysis.

The spectra obtained in the EDX analysis (not shown) confirmed the presence of Ni on the surface of both prepared catalysts. The calculated Ni/Al atomic ratios are reported in Fig. 1: the obtained values varied zone by zone, and resulted higher compared to the theoretical Ni/Al atomic ratios (equal to 0.043 and 0.086 for 5% and 10% Ni/Al_2O_3, respectively), denoting the existence of nickel clusters on the catalyst surface, especially for the 10% one.

H_2 adsorption–desorption isotherms of the commercial crushed and sieved γ-Al_2O_3 (collected fraction 600–1000 μm, the same fraction used to prepare the catalysts) and of the two prepared catalysts displayed type IV isotherms, according to IUPAC classification, with the hysteresis loop typical of mesoporous structures with one dimensional cylindrical channels. The obtained values of BET s.s.a. and BJH p.s.d. are listed in Table 1: a decrease in s.s.a., so as in the p.s.d. values, was observed as the Ni load increased, indicating a partial blockage of the carrier pores, or coverage of the internal surface of pores with reduction of their diameter [30].

Table 1
Morphological characterization of commercial γ-Al_2O_3 and of the Ni-based catalysts.

	γ-Al_2O_3	5% Ni/Al_2O_3	10% Ni/Al_2O_3
BET s.s.a. [$m^2\ g^{-1}$]	133.8	109.2	100.1
BJH pore volume [$cm^3\ g^{-1}$]	0.80	0.72	0.63
BJH pore diameter [nm]	2.4	2.0	1.9
Ni dispersion [%]	–	0.18	0.12

In the XPS analysis Ni 2p core-level spectra of calcined 10% Ni/Al_2O_3 catalyst (Fig. 2) was investigated; the Ni $2p_{2/3}$ binding energy was 856.1 eV (±0.3 eV). Even though the values in the literature for the Ni 2p binding energies are spread over a fairly broad energy interval, the Ni $2p_{2/3}$ obtained value can be assigned to nickel aluminate $NiAl_2O_4$. Moreover, the Ni $2p_{1/2}$–Ni $2p_{3/2}$ splitting of 17.6 eV confirms this assignment, and the presence of strong shake-up satellite structures indicates the presence of Ni(II) ions in a paramagnetic state [31]. In fact, the fresh catalyst particles appeared light blue-green like spinel $NiAl_2O_4$. Therefore, a

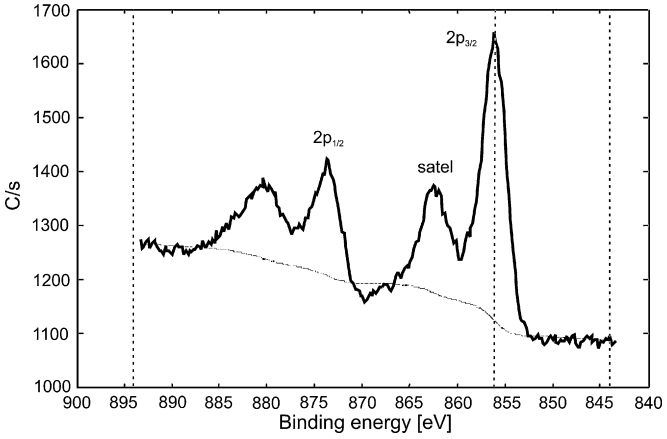

Fig. 2. X-ray photoelectron spectra (Ni 2p region) of 10% Ni/Al_2O_3 catalyst calcined at 900 °C for 2 h.

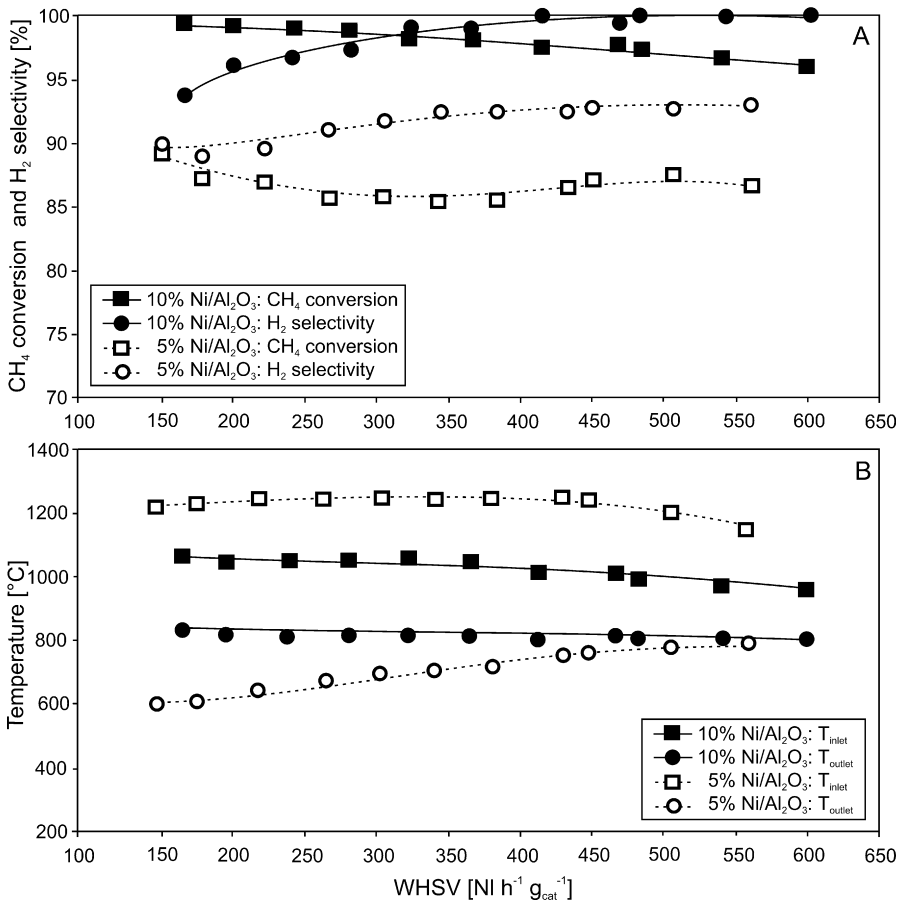

Fig. 3. CH_4 conversion and H_2 selectivity (A), T_{inlet} and T_{outlet} (B) vs. WHSV for the 5% Ni/Al_2O_3 and 10% Ni/Al_2O_3 catalysts. Feed: pure CH_4 and O_2; O_2/CH_4 average ratio of about 0.572 ± 0.005.

spinel $NiAl_2O_4$ structure could be present on the catalyst surface. Moreover, this occurrence can be supported considering the used preparation methods (calcinations at 900 °C for 2 h) which could have created a stronger bonding between Ni and the Al_2O_3 carrier. The "surface spinel" model proposed by Jacono et al. [32], where Ni^{2+} ions occupy the tetrahedral sites in γ-Al_2O_3, again supports this possibility. The wide ranging literature values of the main peaks of nickel oxides suggests also the presence on the surface of NiO, which can be supported by the strong shake-up lines around 860.7 eV ($2p_{3/2}$), indicative of Ni^{2+} species. It is noteworthy that the FWHM value was quite large (3.1 ± 0.1 eV) indicating a surface heterogeneity of the supported Ni, which can be exposed in different ways, from nickel oxide NiO to nickel strongly bonded with the Al_2O_3 carrier as $NiAl_2O_4$. The calculated atomic surface ratio Ni/Al was equal to 0.1, in a good agreement with EDX analysis (0.094 as reported in Fig. 1B). Sahli et al. [33] demonstrated that sub-stoichiometric spinel structures possessed such properties to perform as active catalysts: for Ni/Al atomic ratio lower than 0.5, a solid solution of Al_2O_3 and $NiAl_2O_4$ could develop, characterized by high specific surface area (~105 $m^2\,g^{-1}$).

The XRD spectra of 5% and 10% Ni/Al_2O_3 catalysts (not reported here for sake of space) enlightened the presence of the Al_2O_3 γ phase and the spinel $NiAl_2O_4$, in very good agreement with the XPS analysis results. XPS and XRD results were also in good agreement with the dispersion measurements of Ni for both catalysts determined by CO chemisorption (see Table 1), which disclosed that practically no metallic Ni was present in the samples: most probably all the Ni deposited on the catalysts was chemically bonded with the matrix carrier as spinel.

The results from the experimental test activity carried on all the synthesized catalysts are shown vs. WHSV as CH_4 conversion $(CH_4)_{conv}$ and H_2 selectivity $(H_2)_{sel}$ (Fig. 3A) and as inlet and outlet temperature (T_{inlet} and T_{outlet}) of the fixed bed (Fig. 3B). $(CH_4)_{conv}$ and $(H_2)_{sel}$ were calculated as follows: $(CH_4)_{conv}$ = (inlet CH_4 molar rate − outlet CH_4 molar rate)/(inlet CH_4 molar rate) and $(H_2)_{sel}$ = (outlet H_2 molar rate)/[2 × (inlet CH_4 molar rate − outlet CH_4 molar rate)]. The data in Fig. 3 refer to pure CH_4 and O_2 fed to the reactor; during the tested flow rates, the average O_2/CH_4 ratio was equal to 0.572 ± 0.005 for each tested condition. All the inlet and outlet temperatures and outlet gas stream concentrations data were recorded when the steady-state was reached; the reported data are averaged values since all the tests were repeated two folds. The two catalysts showed excellent performance in the whole examined WHSV range, in particular 10% Ni/Al_2O_3: $(CH_4)_{conv}$ was always higher than 95% and slightly decreased by increasing WHSV for both catalysts, but $(H_2)_{sel}$ increased till values of 100% at the highest flow rates only for 10% Ni/Al_2O_3. This catalyst started with high CH_4 conversion (99.5%) at low WHSV, maintained a very stable trend for all the tested WHSV range and reached the minimum value of 96% at the very high WHSV of 600 Nl h^{-1} g_{cat}^{-1} (corresponding to a gas hourly space velocity GHSV, i.e., the ratio between the reactor volume occupied by the catalyst and the feed flow rate, of about 308,000 h^{-1}).

As concerns the temperatures (Fig. 3B), for both catalysts the T_{inlet} values were always higher than the corresponding ones with an average difference of 200 and 480 °C for 10% Ni/Al_2O_3 and 5% Ni/Al_2O_3, respectively, and with temperatures ranging from 600 to 1200 °C. This $T_{inlet} - T_{outlet}$ difference in the catalytic bed allows

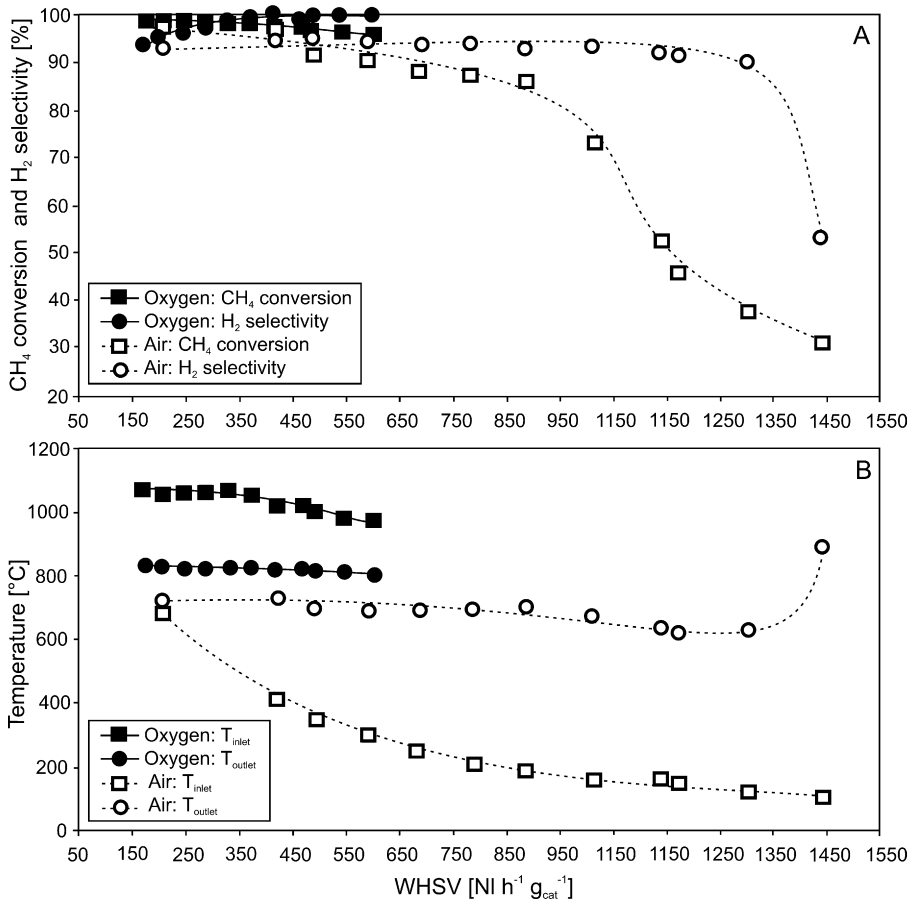

Fig. 4. CH_4 conversion and H_2 selectivity (A), T_{inlet} and T_{outlet} (B) vs. WHSV for the 10% Ni/Al_2O_3 catalyst; experimental runs with CH_4 and pure O_2 or air as feedstock.

supposing the presence and dominance of an indirect mechanism based on the coexistence of two zones: a zone at the catalyst entrance with strongly exothermic CH_4 oxidation to H_2O and CO_2 (combustion zone), followed by a second one where the strongly endothermic steam- and CO_2-reforming reactions were dominant (reforming zone) [9]. Thus the temperature data reflected this situation. For each axial position along catalytic bed if the heat released by methane combustion is higher than the ones removed by the solid–gas heat transfer and absorbed by the endothermic reactions, then an increase of the temperature occurs, otherwise the temperature will go down (endothermic reactions prevailing).

For both catalysts, by increasing WHSV, CH_4 conversion slightly decreased while H_2 selectivity increased, as the result of not only the lower residence time. Increasing the feed flow rate increases the heat transfer along the catalytic bed and if the higher combustion heat released due to the higher CH_4 fed flow is not enough to maintain the same T_{inlet}, the latter becomes lower causing a loss of performance towards CH_4 conversion. On the other hand, an increase in gas flow rate improves the mass transfer to the catalytic surface and especially the heat and mass transport among adjacent combustion and reforming zones, thus favouring the endothermic reactions; this can explain the increase in H_2 selectivity with WHSV. At very high space velocity the combustion zone can move towards the bed outlet or leave tumbling the performance in syngas production or, at worst, cause the reactions shutdown; the WHSV value governing the reactor shut-off depends on the activity of catalysts towards CH_4 CPO reactions.

Fig. 4 compares the 10% Ni/Al_2O_3 catalyst activity when working with pure O_2 with that obtained with air using the same start-up procedure and working conditions. For both the test runs the potential thermal power input of the reactor was the same, i.e., the fed CH_4 flow rate was identical during the tests with O_2 or air. The slightly higher (about 6%) O_2/CH_4 ratio (0.606 ± 0.008) kept for the run with air compared to the one used with O_2 (0.572 ± 0.005) was adopted to increase the heat released during the methane oxidation to somehow try to compensate the 2.9 folds larger total mass flowing through the reactor, due to the presence of N_2, without affecting in a too negative way the reactor performance. The inert gas was moreover responsible for the higher values of WHSV obtained during the tests with air, as also for the dilution of the reacting gases and the lower temperature level in the catalytic bed. With the adopted conditions, at low WHSV $(CH_4)_{conv}$ using air was very high (equal to 98.6%), a value very close to the one obtained with pure O_2. $(CH_4)_{conv}$ remained at high values (>90%) till a WHSV value of 600 Nl h^{-1} $g_{cat}{}^{-1}$ (GHSV ≈ 308,000 h^{-1}). Therefore, the reactor performance using air was satisfactory and only slightly lower compared to the obtained performance using O_2. However, at higher WHSV values the axial heat transfer along the bed prevailed compared to the combustion heat generation, resulting thus in a key reduction of $(CH_4)_{conv}$ until 31% at WHSV equal to 1440 Nl h^{-1} $g_{cat}{}^{-1}$ (GHSV ≈ 750,000 h^{-1}). The $(H_2)_{sel}$ curve had, instead, a very different trend by increasing WHSV: it began with values higher than 90%, remained stable until 1300 Nl h^{-1} $g_{cat}{}^{-1}$ (GHSV ≈ 680,000 h^{-1}) and then dropped to 53.5%. The test with air presented an average lower thermal level compared to those with pure O_2: the recorded temperatures, in fact, presented opposite trends (see Fig. 4B). Despite the same potential power input provided by the fed CH_4, when air was used T_{inlet} and T_{outlet} were significantly lower compared to the recorded temperatures with pure O_2, due to the presence of N_2 as diluting agent. Moreover, with

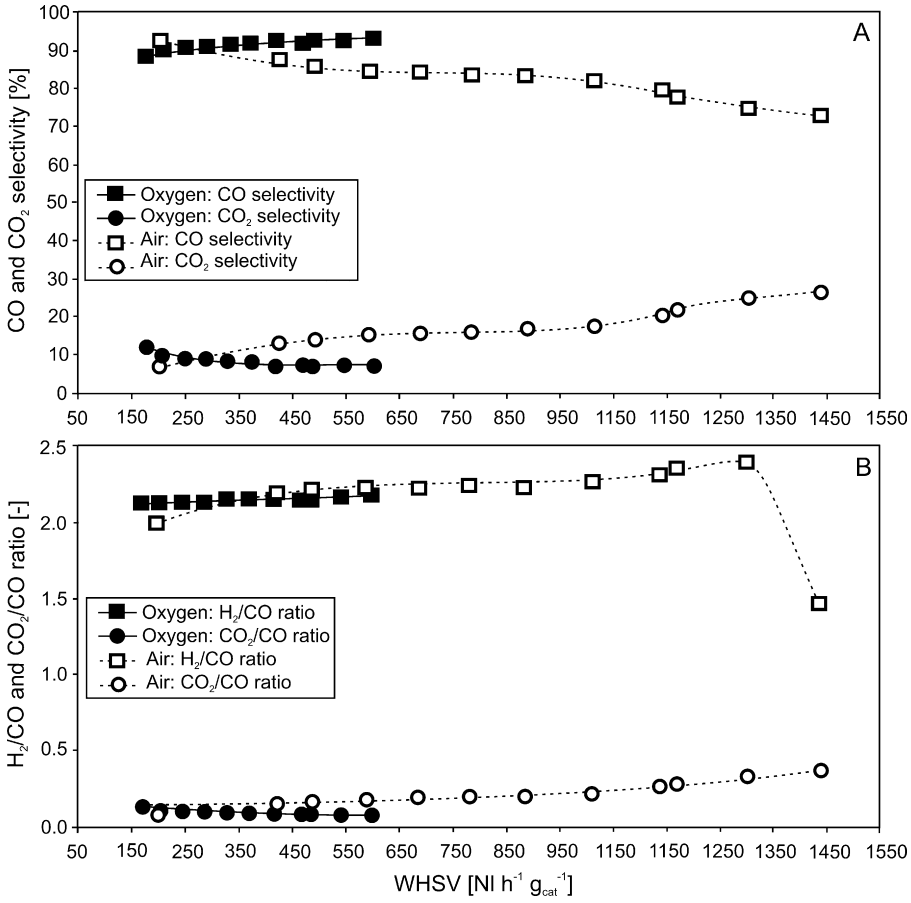

Fig. 5. CO and CO_2 selectivity (A), H_2/CO and CO_2/CO ratios (B) vs. WHSV for the 10% Ni/Al_2O_3 catalyst; experiments run with CH_4 and pure O_2 (O_2/CH_4 average ratio of about 0.572 ± 0.005) or air (O_2/CH_4 average ratio of about 0.606 ± 0.008) as feedstock.

air T_{inlet} was always lower than the corresponding T_{outlet}, whereas with O_2 an opposing situation was always recorded (T_{inlet} always higher than the corresponding T_{outlet}). When working with air, the inlet feedstock preheating by back-radiation/conduction reached lower values for both the larger mass rate and the lower residence time. Consequently, at very high flow rate, i.e., at very short contact time, due to the presence of N_2 the combustion zone progressively moved downward along the bed pushing the endothermic reactions at the end of the catalytic region. T_{inlet}, in fact, continuously decreased since the combustion zone shifted downward, reducing thus the possibility to heat-up the gas feed, now carrying also the diluting N_2. The endothermic reactions progressively shut-down led additional heat to remain in the bed and be employable by the gas phase, so balancing the increased heating necessities of the flowing gas mass rate and maintaining T_{outlet} at the same value. The latter showed a rapid rise (see Fig. 4) only at the highest WHSV value, when the thermal energy balance shifted favouring the system heating. Anyway, the reactor provided a performance similar to the one when working with pure O_2 (obviously the obtained syngas was diluted due the presence of N_2) till about a WHSV value of 600 Nl h^{-1} g_{cat}^{-1} and remained thermally self-sustained using air rather than pure O_2 for each tested WHSV until to 1440 Nl h^{-1} g_{cat}^{-1} (GHSV $\approx$ 750,000 h^{-1}).

To better understand the reaction mechanisms in the SCT-CPO reactor, also the CO and CO_2 selectivity and the H_2/CO and CO_2/CO molar flow rate ratios were considered, as reported in Fig. 5. The CO and CO_2 selectivity were calculated as: $(CO)_{sel}$ = (outlet CO molar rate)/(inlet CH_4 molar rate − outlet CH_4 molar rate) and $(CO_2)_{sel}$ = (outlet CO_2 molar rate)/(inlet CH_4 molar rate − outlet CH_4 molar rate). $(CO)_{sel}$ and $(CO_2)_{sel}$ trends were opposite and in accordance with the temperature trends (see Figs. 4B and 5A): with pure O_2, $(CO)_{sel}$ increased and $(CO_2)_{sel}$ decreased by increasing WHSV, whereas with air $(CO)_{sel}$ decreased and $(CO_2)_{sel}$ increased by increasing WHSV, sign that with O_2 the CO concentration, whereas with air the CO_2 concentration, respectively increased with WHSV. This was also evident by the CO_2/CO ratio reported in Fig. 5B. Such trends could suggest that working with pure O_2, the dry reforming should be the main reaction in producing the syngas, whereas the steam reforming should be the prevailing reaction when air was used.

The H_2/CO ratio (equal to 2 if only the direct partial oxidation reaction occurs) was almost constant at ~2.15 for the tests with pure O_2, whereas for the tests with air it increased from ~2 to ~2.4, sign that the H_2 formation was prevailing on the CO one. The higher H_2/CO values recorded with air were in line with the hypothesis that the steam reforming reaction should prevail when working with air (H_2/CO = 3 if only the steam reforming occurs) and the dry reforming reaction should prevail when working with pure O_2 (H_2/CO = 1 if only the dry reforming takes place).

Therefore, the presence of N_2 in the feedstock had a negative effect on CH_4 conversion and syngas selectivity at very short contact time (high WHSV values), as demonstrated also by other authors [7]. This could be explained considering that both the reduced overall thermal level of the reactor and the diluting effect on the reactant gas concentrations for the N_2 presence affected detrimentally the system kinetics. On the contrary, the higher both temperature and reactant concentrations played favourably on the overall kinetics of syngas production when working with pure O_2 [15]. Conversely, working with air presents some advantages, mainly in terms of management costs of the process (O_2 must not be separated by

N_2: this could be very useful for ammonia synthesis, for example). Moreover, thanks to the lower thermal level of the system, the catalyst results less thermally stressed, allowing longer lifetime and better resistance to sintering effects.

4. Conclusions

Catalytic partial oxidation of methane in SCT reactor offers an advantageous and promising alternative to steam reforming for syngas production. The present work investigated the activity performances of low cost nickel based catalysts over γ-Al_2O_3 (5% and 10% by weight as nickel load) towards syngas production in thermally self-sustained reactor at very high space velocity using pure O_2 at first and then air. In the tests with pure O_2, 10% Ni/Al_2O_3 catalyst showed the best performance towards CH_4 conversion and H_2 selectivity due to the larger Ni load on Al_2O_3 support with excellent conversion always higher than 95% and H_2 selectivity of 100% at high WHSV values and maintained stable and almost constant T_{inlet} and T_{outlet} in all the tested WHSV, never exceeding 1200 °C. The tests with air with the same methane fed flow rate strongly increased the WHSV, but CH_4 conversion starting from value similar to that obtained with oxygen at low WHSV, firstly decreased slowly till WHSV of about 600 Nl h^{-1} $g_{cat}{}^{-1}$, then strongly till a minimum value of about 30%. The H_2 selectivity remained almost constant up to WHSV of 1300 Nl h^{-1} $g_{cat}{}^{-1}$ (GHSV ≈ 680,000 h^{-1}); for higher WHSV values the combustion zone moved towards the end of the bed causing a fall down of the CPO performance and an increase of T_{outlet}. Anyway, 10% Ni/Al_2O_3 was able to maintain the reactor thermally self-sustained using air rather than pure O_2 until GHSV ≈ 750,000 h^{-1} and gave a performance similar to that with pure O_2 (but producing a syngas diluted from N_2) till a WHSV value of 600 Nl h^{-1} $g_{cat}{}^{-1}$.

References

[1] J.N. Armor, Appl. Catal. A 176 (1999) 159.
[2] L. Carrette, K.A. Friedrich, U. Stimming, Fuel Cells 1 (2001) 5.
[3] V.R. Choudhary, A.M. Rajput, V.H. Rane, Catal. Lett. 16 (1992) 269.
[4] V.R. Choudhary, V.H. Rane, A.M. Rajput, Appl. Catal. A: Gen. 162 (1997) 235.
[5] A.T. Ashcroft, P.D.F. Vernon, M.L.H. Green, Nature 344 (1990) 319.
[6] D. Dissanayake, M.P. Rosynek, K.C. Kharas, J.H. Lunsford, J. Catal. 132 (1991) 117.
[7] B.C. Enger, R. Lødeng, A. Holmen, Appl. Catal. A: Gen. 346 (2008) 1.
[8] D.A. Hickman, L.D. Schmidt, Science 259 (1993) 343.
[9] L.D. Schmidt, M. Huff, Catal. Today 21 (1994) 443.
[10] R. Horn, K.A. Williams, N.J. Degenstein, A. Bitsch-Larsen, D. Dalle Nogare, S.A. Tupy, L.D. Schmidt, J. Catal. 249 (2007) 380.
[11] A.S. Bodke, S.S. Bharadwaj, L.D. Schmidt, E. Ranzi, Science 285 (1999) 712.
[12] O. Deutschmann, L.D. Schmidt, AIChE J. 44 (1999) 2465.
[13] D.K. Zerkle, M.D. Allendorf, M. Wolf, O. Deutschmann, J. Catal. 196 (2000) 18.
[14] L. Basini, K. Aasberg-Petersen, A. Guarinoni, M. Ostberg, Catal. Today 64 (2001) 9.
[15] K.L. Hohn, L.D. Schmidt, Appl. Catal. A: Gen. 211 (2001) 53.
[16] I. Tavazzi, A. Beretta, G. Groppi, P. Forzatti, Stud. Surf. Sci. Catal. 147 (2004) 163.
[17] I. Tavazzi, A. Beretta, G. Groppi, P. Forzatti, J. Catal. 241 (2006) 1.
[18] J.B. Claridge, M.L.H. Green, S.C. Tsang, A.P.E. York, A.T. Ashcroft, P.D. Battle, Catal. Lett. 22 (1993) 299.
[19] A.P.E. York, T.C. Xiao, M.L.H. Green, Top. Catal. 22 (2003) 345.
[20] W.Z. Weng, C.R. Luo, J.J. Huang, Y.Y. Liao, H.L. Wan, Top. Catal. 22 (2003) 87.
[21] Platinum Today, Johnson Matthey, London, 2010 (Sept.), www. platinum.matthey.com.
[22] S. Wang, G.Q. Lu, Appl. Catal. A 169 (1998) 271.
[23] L. De Rogatis, T. Montini, A. Cognigni, L. Olivi, P. Fornasiero, Catal. Today 145 (2009) 176.
[24] Y. Zhang, G. Xiong, S. Sheng, W. Yang, Catal. Today 63 (2000) 517.
[25] Z.-W. Liu, K.-W. Jun, H.-S. Roh, S.-C. Baek, S.-E. Park, J. Mol. Catal. A: Chem. 189 (2002) 283.
[26] H. Özdemir, M.A.F. Öksüzömer, M.A. Gürkaynak, Int. J. Hydrogen Energy 35 (2010) 12147.
[27] J.A. Villoria, M.C. Alvarez-Galvan, R.M. Navarro, Y. Briceño, F. Gordillo Alvarez, F. Rosa, J.L.G. Fierro, Catal. Today 138 (2008) 135.
[28] S. Specchia, G. Negro, G. Saracco, V. Specchia, Appl. Catal. B: Environ. 70 (2007) 525.
[29] S. Specchia, L.D. Vella, B. Lorenzut, T. Montini, V. Specchia, P. Fornasiero, Ind. Eng. Chem. Res. 49 (2010) 1010.
[30] A.L. Alberton, M.M.V.M. Souza, M. Schmal, Catal. Today 123 (2007) 257.
[31] B.W. Hoffer, A.D. van Langeveld, J.P. Janssens, R.L.C. Bonné, C.M. Lok, J.A. Moulijn, J. Catal. 192 (2003) 432.
[32] M.L. Jacono, M. Schiavello, A. Cimino, J. Phys. Chem. 75 (1971) 1044.
[33] N. Sahli, C. Petit, A.C. Roger, A. Kiennemann, S. Libs, M.M. Bettahar, Catal. Today 113 (2006) 187.